DOI 10.1002/biot.201100181 Biotechnol. J. 2012, 7, 428–439

Research Article

Integrated biofabrication for electro-addressed in-film bioprocessing

Jessica L. Terrell[1,2], Tanya Gordonov[1,2], Yi Cheng[3], Hsuan-Chen Wu[1,2], Darryl Sampey[1,4], Xiaolong Luo[2], Chen-Yu Tsao[2], Reza Ghodssi[5], Gary W. Rubloff[3,6], Gregory F. Payne[1,2] and William E. Bentley[1,2]

[1] Fischell Department of Bioengineering, University of Maryland, College Park, MD, USA
[2] Institute for Bioscience and Biotechnology Research, University of Maryland, College Park, MD, USA
[3] Institute for Systems Research, University of Maryland, College Park, MD, USA
[4] BioFactura, Inc., Key West Ave, Rockville, MD, USA
[5] Department of Electrical and Computer Engineering, University of Maryland, College Park, MD, USA
[6] Department of Materials Science and Engineering, University of Maryland, College Park, MD, USA

Many recent advances in bioprocessing have been enabled by developments in miniaturization and microfluidics. A continuing challenge, however, is integrating multiple unit operations that require distinct spatial boundaries, especially with included labile biological components. We have suggested "biofabrication" as a means for organizing cells and biomolecules in complex configurations while preserving function of individual components. Polysaccharide films of chitosan and alginate that are assembled on-chip by electrodeposition are "smart" configurable interfaces that mediate communication between the biological systems and microfabricated devices. Here, we demonstrate the scalable performance of a *production* address, where incubated cells secrete antibodies, and a *capture* address, where secreted antibody is retained with specificity and subsequently assayed. The antibody exchange from one electro-address to another exemplifies integrated in-film bioprocessing, facilitated by the integrated biofabrication techniques used. This in-film approach enables complex processes without need for microfluidics and valving. Finally, we have shown scalability by reducing electrode sizes to a 1 mm scale without compromising film biofabrication or bioprocessing performance. The in situ reversible deposition of viable cells, productivity characterization, and capture of secreted antibodies could find use in bioprocessing applications such as clonal selection, run-to-run monitoring, initial scale-up, and areas including drug screening and biopsy analysis.

Received	22 JUL 2011
Revised	14 NOV 2011
Accepted	22 DEC 2011
Accepted article online	28 DEC 2011

Keywords: Antibody exchange · Biofabrication · Calcium alginate · Chitosan · Electrodeposition

1 Introduction

Advances in microsystems technologies have revolutionized the study of biology by allowing rapid and parallel analysis of micro and nanoliter samples; they have also enabled a reexamination of bioprocessing [1–3]. Virtually all bioprocess operations have been tapered to significantly smaller length scale [4, 5]. Both on-chip and fluidics-based systems have appeared for a variety of tasks, many of which are now commercial products (e.g., DNA microarrays, DNA amplification, fermentation, and molecular separations) [6–12]. Systems that integrate two or more operations are less common, however, in part because the spatial arrangement of various biological components within these mi-

Correspondence: Dr. William E. Bentley, Fischell Department of Bioengineering, University of Maryland, College Park, MD 20742, USA
E-mail: bentley@umd.edu

Abbreviations: **$CaCl_2$**, calcium chloride; **$CaCO_3$**, calcium carbonate; **DI**, deionized; **DPBS**, Dulbecco's PBS; **f_v**, fraction viable; **HG3T**, engineered protein G; **IgG**, immunoglobulin G; **ITO**, indium tin oxide; **TPP**, tri-polyphosphate

Colour online: See the article online to view the figures in colour.

crosystems remains a challenge [13–15]. Fabrication processes must allow for spatial organization of fragile biological components while preserving functionality. In addition, systems integration concepts that ensure valving and microactuators reliably distribute various fluid components to specific locales increase complexity both at the design and fabrication stages.

We have proposed biofabrication as a strategy to address this challenge [16]. Specifically, we employ electrodeposited polysaccharide films to facilitate the spatial assembly of relevant biomolecules and cells on-chip and within fluidic microsystems [17–20]. Polysaccharide films serve as biocompatible interfaces with unique suitabilities [15]. Because they are stimuli responsive and because the stimuli (pH, temperature) can be signaled using microelectronics, their assembly and functionality can be "programmed" with high spatial resolution [20–23]. Then, because a particular bioprocess operation of interest is associated with the polysaccharide electrodeposited at a specific site, programmed assembly of multiple bioprocess operations should be enabled. In our recent work, we assembled yeast in alginate and agarose, induced antigen-specific binding variable lymphocyte receptors (VLRs) on their outer surfaces, then demonstrated an on-chip immunoassay of the receptor-ligand binding [24]. All operations took place at a single location on a chip. In our current work, we demonstrate electro-addressing of antibody-secreting NS0 cells within alginate-based hydrogels after assembling an antibody capture surface in an adjacent register. All components are surface addressed on-chip to enable rapid and simple "in-film" bioprocessing. The electro-addressability of film interfaces facilitates the proximal placement of multiple biological functionalities, conferring greater complexity in interactions by their integration. Additionally, after demonstrating the process integration, we miniaturized the system to millimeter-scaled registers while preserving function.

Central to our concept is a spatially mindful design for molecular exchange between electrode addresses. In Fig. 1A, we have envisioned a biofabricated polysaccharide-based environment for in-film bioprocessing events. Alginate has known utility as a cell-entrapping scaffold [25, 26]. Here, an electrodeposited alginate film assembles and houses cells at a *production address*; metabolic products, notably mAbs, are secreted from this address. Adjacently, a *capture address* is biofabricated using a chitosan film functionalized with engineered protein G (HG3T) molecules through fusion tag tethering [18]. With protein G functionality, this address becomes receptive to the Fc portion of antibodies, and in this application, recovers those generated at the production address [18, 27–29].

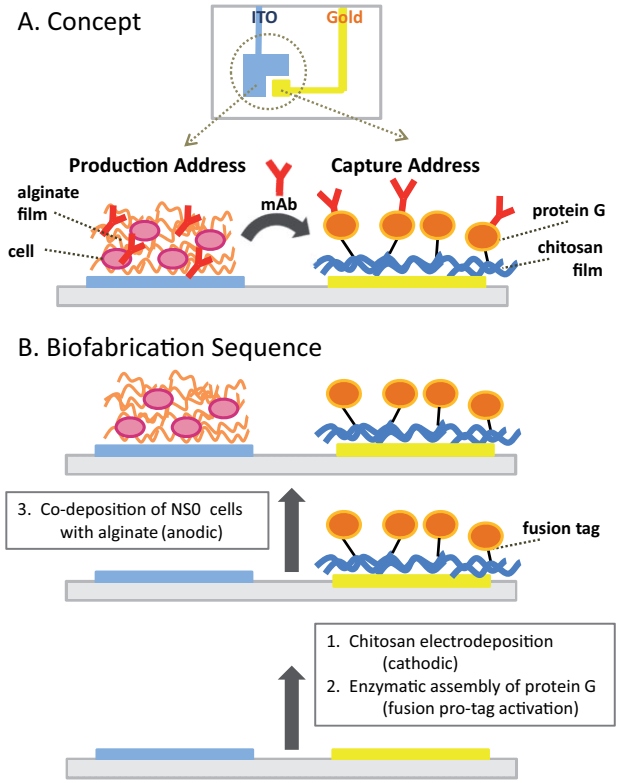

Figure 1. Integrated biofabrication. (**A**) In-film bioprocessing is facilitated by the electro-addressing of alginate and chitosan films onto adjacent ITO and gold electrodes. Film biofabrication achieves a cell-entrapped alginate film and protein G functionalized chitosan film. Once assembled at neighboring addresses, cells secrete antibodies, which may diffuse and bind to protein G. (**B**) Integrated biofabrication occurs by sequential assembly. First, gold is cathodically biased to electrodeposit chitosan, followed by enzymatic assembly of protein G onto chitosan, using tyrosinase to activate a pro-tag engineered onto the protein. Then, transfectant NS0 cells are co-deposited with alginate by anodically biasing the ITO electrode in the presence of $CaCO_3$ to release calcium ions for crosslinking.

Figure 1B outlines an integrated biofabrication procedure for sequential assembly of the production and capture addresses. Procedures for our work explored capture address assembly followed by production address assembly, as depicted in Fig. 1B. Our capture address is created using an aqueous solution containing chitosan pipetted onto microfabricated chips with patterned electrode pairs (one being indium tin oxide (ITO) and the other gold). Locally, at a negatively biased electrode (gold), chitosan's primary amines become deprotonated, allowing film formation at the electrode surface [21]. In our previous work, we demonstrated chitosan film conjugation by enzymatic assembly of an HG3T that is modified to contain a tyrosine

rich "pro-tag" [18, 30]. Enzymatic "activation" of the tag's tyrosine residues via tyrosinase, enables covalent coupling of the resultant quinone to the primary amines on deposited chitosan [31–33]. The tyrosinase activation reaction is depicted below:

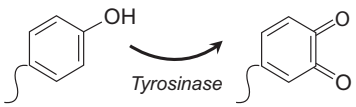

HG3T is then a binder with specificity for the Fc region on freely suspended immunoglobulin G (IgG), and when coupled to chitosan, creates a capture address (Fig. 1B).

Then, shown in Fig. 1B, a solution containing NS0 cells, alginate and calcium carbonate ($CaCO_3$) is applied on-chip, where an optically-neutral positively-biased electrode (ITO) is proximal to the chitosan film. During conventional alginate gel formation, alginate chelates calcium ions to form crosslinks between chains [25]. In our strategy, the hydrolysis of water at the electrode (low pH) releases calcium ions and liberates carbon dioxide from the $CaCO_3$, yielding a cell-entrapped alginate hydrogel overlaid onto the electrode with identical dimensions [34]. The cells used here are an NS0 myeloma cell line, transfected to produce a monoclonal IgG (mAb) recognizing the vaccinia virus L1 protein. Contingent on remaining viable, the co-deposited productive NS0 cells comprise the production address. In our previous studies, eukaryotic yeast cells were entrapped by alginate electrodeposition and remained viable [24].

Of note, alginate hydrogel formation is reversible, subject to the presence of a calcium chelator such as citrate. That is, addition of citrate should dissolve these alginate films, presumably with minimal effect on cell metabolism [35]. Exploiting this reversible containment attribute, mAbs that were retained within the alginate film could be liberated into solution along with cells by introducing citrate. This potentially allows for both screening production capability and subsequent recovery of assembled cells. In this paper, we demonstrate the creation of both addresses and their utility; we also demonstrate reversibility of cell capture for culture scale-up.

2 Materials and methods

2.1 Instrumentation

A Keithley 2400 SourceMeter was used for electrodeposition and platinum foil was used as a counter electrode. Olympus imaging technologies were used: an MVX10 MacroView fluorescecence stereomicroscope for electrode and cell imaging and a DP72 camera with CellSens Standard software. Mean gray value measurements of electrode fluorescence and immunoassay signals were evaluated with ImageJ software. ELISA results were obtained with a SpectraMax M2e microplate reader and SoftMax Pro 5.3 software from Molecular Devices. FACS analyses were performed using a BD FACSCanto II flow cytometer and BioFACS Diva software for data collection by BD Biosciences.

2.2 Electrode fabrication

Metal electrodes were coated onto a silicon wafer by thermal evaporation of 12 nm of chromium (Cr) and 120 nm of gold (Au). Standard photolithography and subsequent etching of Cr and Au were performed to define pairs of electrodes with 1 mm separation. Each active rectangular electrode (1 mm × 4 mm) is connected to a contact pad via a thin contact lead (200 μm in width). Electrodes were physically separated using a microdicing saw.

To create adjacent ITO and gold electrodes (shown in Figs. 2A, 4A), photolithography and etching were performed on an ITO coated glass slide (Sigma-Aldrich) to define "L-shaped" ITO electrodes. Second, the gold electrodes were defined by additional photolithography, thermal evaporation (12 nm of Cr and 120 nm of Au) and lift-off. See Table 1 for electrode dimensions.

2.3 Solution preparation

A solution of 2% alginate was prepared by autoclaving a mixture of alginate (Sigma-Aldrich, medium viscosity) and 1% $CaCO_3$ (Specialty Minerals, MultiFex MM 70 nm particles) suspended in deionized (DI) water to sterilize and promote dissolution, then subjecting the solution to continuous stirring. Green fluorescently labeled alginate was prepared by adding 1 μL/mL of FluoroSpheres (Invitrogen, F8765) amine-modified fluorescent microspheres (1 μm diameter, Ex/Em: 505:515) to the alginate solution and vortexing for 1 min. The chitosan used was isolated from crab shells and at least 85%

Table 1. Scalable electro-address dimensions

Electrode pair	Capture area (CA) (mm^2 gold)	Production area (PA) (mm^2 ITO)	PA/CA
Large	9	33	3.67
Medium	4	16	4
Small	1	4	4

ITO and gold electrode pairs were fabricated in three sizes, with nearly equivalent surface area ratios between the production address (on ITO) and the capture address (on gold).

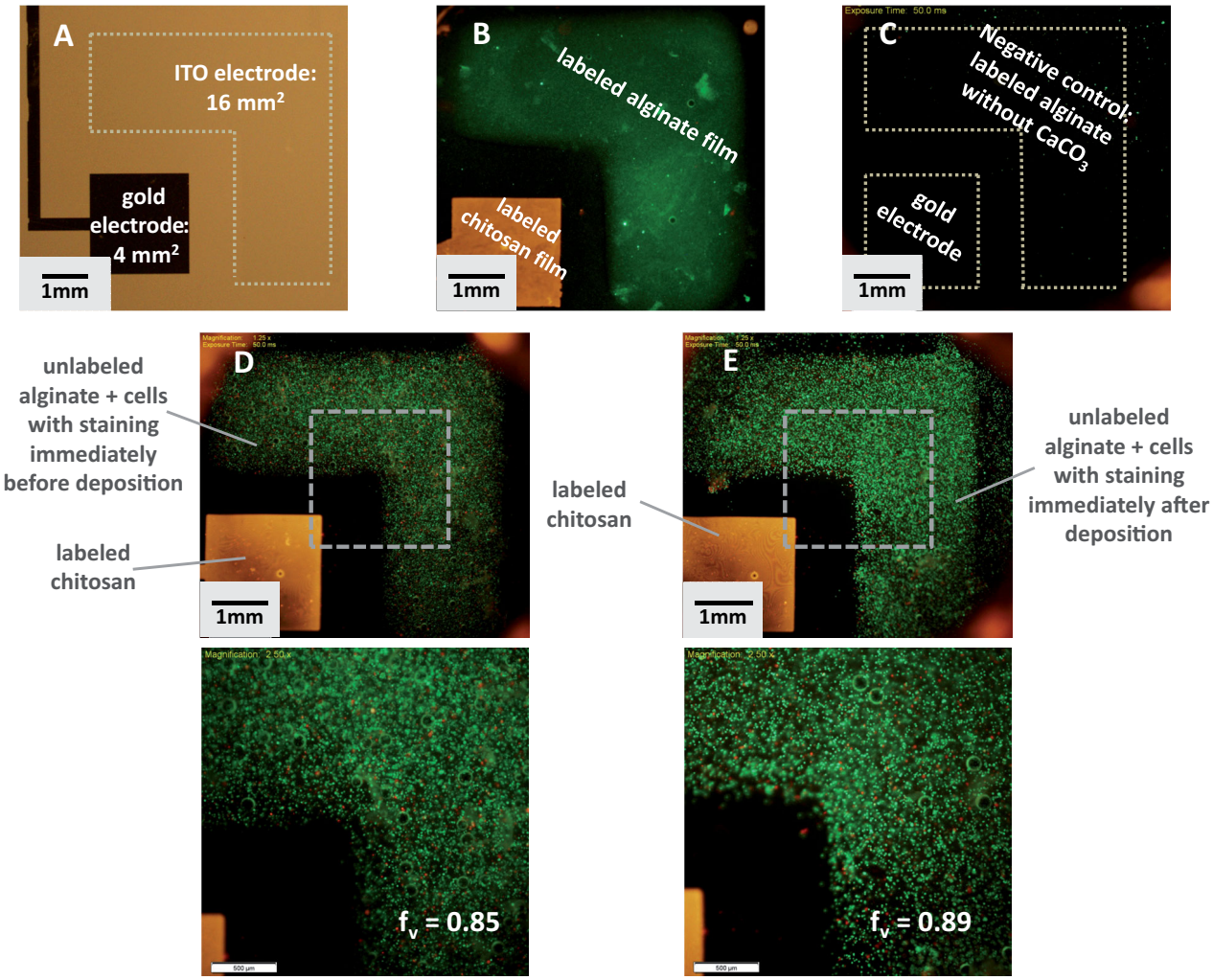

Figure 2. Electro-addressability of sequentially deposited and cell-entrapped films. (**A**) Brightfield image of patterned electrodes prior to film electrodeposition. (**B**) Fluorescence image of red-labeled chitosan deposited on gold followed by green-labeled alginate deposited on ITO by localized calcium release from $CaCO_3$. (**C**) Fluorescence image showing a gold electrode with the absence of a chitosan film and a negligible presence of labeled alginate when deposited without $CaCO_3$. (**D**) Cells were stained for viability (green = live; red = dead) *before* co-depositing on ITO with alginate. The viable fraction (f_v) is representative of the cell culture viability, 0.85. Cells remained immobilized throughout washing steps. (**E**) Cells were stained for viability *after* co-depositing with alginate; the f_v is 0.89. Data depicted are representative of triplicate experiments.

deacetylated (Sigma-Aldrich). Chitosan was prepared by dissolving at a low pH (~3) and then adjusting the pH to ~5 with NaOH. The final concentration was 1.6% and was further adjusted to 0.5% in DI water for electrodeposition. Red fluorescently labeled chitosan was prepared according to Wu et al., 2003 using 5-(and-6)-carboxyrhodamine 6G succinimidyl ester (Ex/Em: 525:560, Invitrogen) [36].

2.4 Cell culture

The cells used were provided courtesy of Darryl Sampey (Biofactura, Inc.). Briefly, an NS0 myeloma cell line had been transfected by electroporation to produce a chimeric IgG1 antibody that is monoclonal against vaccinia virus protein L1. Stably transfected cells were isolated using a proprietary metabolic selection strategy that exploits cholesterol auxotrophy of the parental line. The stable pool of transfected cells was cloned two times by limiting dilution to isolate the high expressing subclone. Cells were incubated in Gibco CD hybridoma medium supplemented with MEM non-essential amino acids and L-glutamine (Invitrogen).

2.5 Cell staining

A Live/Dead Viability/Cytotoxicity kit (Invitrogen Molecular Probes) was prepared according to protocol in Dulbecco's PBS (DPBS, Invitrogen) and ap-

plied to the cells for 30 min. For observing stained cells in solution, the cells collected by centrifugation for 5 min at 500 g, resuspended in DPBS to rinse off excess staining solution, and centrifuged again prior to imaging. For staining cells entrapped within an alginate film, the film was briefly rinsed with DPBS prior to imaging. Cell counting by ImageJ analysis was performed on fluorescence images taken separately with FITC and TRITC filter sets and merged for presentation.

2.6 HG3T assembly and antibody capture

HG3T expression and purification in *Escherichia coli* BL21 (DE3) has been described previously [18]. To prepare the chip surface for antibody capture, each electrode was electrodeposited using a solution of 0.4% chitosan in DI water. A cathodic bias of 3 A/m^2 was applied to each gold electrode for 2 min followed by a rinse in DI water. To enzymatically assemble HG3T, the electrodes were incubated overnight at 4°C with 0.4 μM HG3T and 50 U/mL tyrosinase from mushroom (Sigma-Aldrich). Next, 0.2% sodium cyanoborohydride (Sigma-Aldrich) was applied for 15 min, followed by 1% sodium tripolyphosphate (TPP) for 15 min. Electrodes were blocked in 5% dry non-fat milk in PBS for 4 h, then incubated with a standard dilution in 1% milk-PBS + 0.05% Tween or a sample for 2 h. As a secondary label, FITC-conjugated AffiniPure F(ab′)$_2$ fragment goat anti-human IgG (Jackson Immuno Research Laboratories) was applied in 1% milk-TPBS for 2 h. Washing steps were performed in between. For each electrode comparison, identical magnification and fluorescence exposure times were used.

2.7 Cell co-deposition and in-film bioprocessing at the production address

Cells were taken from culture and collected by centrifugation at 500 g for 5 min, resuspended in DPBS to remove superfluous extracellular mAbs, and centrifuged again. Samples were resuspended in DPBS at 20 × 10^6 cells/mL and then an equal volume of 2% alginate and 1% $CaCO_3$ was mixed in to achieve a final concentration of 1% alginate, 0.5% $CaCO_3$, and 10 × 10^6 cells/mL. Approximately 75, 150, or 250 μL of the mixture was applied to each respective small, medium, or large electrode pair, and the cells were allowed to settle on the chip surface for 5 min. An anodic bias of 3 A/m^2 was applied to each ITO electrode for 2 min followed by gentle rinsing of each film with 0.145 M NaCl. Ten millimolar $CaCl_2$ was briefly applied to the films for crosslink densification with subsequent NaCl rinses. Culturing media supplemented with 10 μg/mL gentamicin (Invitrogen) and 500 μM $CaCl_2$ was added for incubation and samples were covered with Breathe-Easy film (Diversified Biotech). After incubating for approximately 5 h at 37°C, production address films were dissolved by applying minimal volumes of 0.2 M sodium citrate and gentle pipetting. Equal volumes of DPBS were added to improve isotonicity and the samples were centrifuged at 500*g* for 5 min to recover suspended cells. Supernatants, presumably containing secreted mAbs, were applied to corresponding capture addresses for 2 h, followed by additional blocking at 4°C to minimize non-specific binding, and finally application of a labeling antibody (see HG3T assembly and antibody capture methods) for fluorescence imaging. Variations of the antibody capture step were reported in our results.

2.8 ELISA standard curve

Standards of comparison were prepared between on-chip and conventional ELISA techniques. Human IgG (Sigma-Aldrich) was prepared in serial dilutions up to 5500 ng/mL. An ELISA was performed using an anti-human IgG alkaline phosphatase conjugate (Sigma-Aldrich) as a secondary antibody and PNPP (Thermo Scientific) as the enzymatic substrate for detection.

3 Results and discussion

3.1 Adjacent electro-addressability of chitosan and alginate films

In Fig. 1, we hypothesized that chitosan and alginate could be electrodeposited sequentially and adjacently with minimal crosstalk or interference between electrode addresses. In Fig. 2A, a bare electrode pair is depicted to demonstrate neighboring gold and ITO geometries. First, a red fluorescently labeled chitosan solution (0.5%) was electrodeposited on a gold electrode (Fig. 2B). Excess solution was rinsed from the film, and a 1% sodium TPP solution was applied to electrostatically reinforce the chitosan film. Second, an alginate (green-fluorescently labeled, see Section 2) and $CaCO_3$ mixture was applied and electrodeposited onto a neighboring ITO electrode. Afterward, the films were rinsed and post-deposition calcium chloride ($CaCl_2$) solution was briefly applied. A fluorescence image was taken of the resulting electrodes, showing that both films were intact (Fig. 2B). A control image is also shown in Fig. 2C where we imaged a pair of electrodes through fluorescence filters after

an alginate deposition procedure in which $CaCO_3$ was absent. In this case, we demonstrate negligible background fluorescence and an inability of alginate to electrodeposit without the presence of $CaCO_3$ (Fig. 2C), thereby indicating its necessity. Also of note, this assembly is evaluated for cross-talk or electrostatic interactions that occur between chitosan and alginate due to their respective net positive and negative charges [37, 38]. Direct application of dissolved alginate on a chitosan film could potentially result in the formation of an electrostatically bound alginate layer on the film's surface [39]. Our application of TPP prior to alginate served to avert such an interaction. Because the overlaid fluorescence image did not show colocalization of the green and red films (Fig. 2B), these electrostatic interactions were minimized.

Next, we monitored cell electro-addressing during the deposition process. In Fig. 2D, chitosan was deposited as mentioned. Cells were stained with a viability/cytotoxicity stain (Live/Dead, Invitrogen); providing visualization and viability assessment. These stained cells were then rinsed, centrifuged, and resuspended to a density of 10×10^6 cells/mL in a solution of 1% alginate and 0.5% $CaCO_3$ in DPBS. Cells were then introduced onto the chips and co-deposited on ITO. The fluorescence image (Fig. 2D) shows that cells were successfully electro-addressed to the ITO electrode. Additionally, the cell population used, stained upon sampling from culture, appeared healthy (live cells fluoresce green while dead cells are red). By image analysis, green and red fluorescence was quantified to determine the fraction viable ($f_v = 0.85$).

On a test ITO electrode, cells were again co-deposited with alginate as described, but were probed for viability after deposition. An identical cell sample was suspended at 10×10^6 cells/mL in a deposition solution. Alginate deposition was performed as described, followed by application of the Live/Dead stain. The fluorescence image (Fig. 2E) again shows an electrodeposited healthy cell population ($f_v = 0.89$). Figure 2E has significance in that it demonstrates co-deposition of NS0 cells without negative impact on cell viability; quantified viabilities between Fig. 2D and E are nearly the same (0.85 and 0.89, respectively).

3.2 Rapid monitoring of mAb production from NS0 cells

Our next set of studies demonstrates rapid and simple on-chip entrapment of cells. Moreover, because the process is simple and rapid we hypothesize these procedures may enable interrogation of cell productivity over time for a full scale production process.

3.2.1 Production address characterization and scalable assembly

We were aware that many parameters may affect the electrodeposited cell density in-film and sought to determine electrodeposition conditions that would ensure uniform and reproducible populations. While many factors were varied, we report here the electrodeposited cell number as a function of cell seeding density, cell "settling" time (duration between loading cell sample and biasing the electrode), film volume, and the electrode surface area. Results are depicted in Fig. 3A. For each parameter tested, data were obtained by first co-depositing cells with alginate on each electrode keeping all other conditions constant (conditions, except when varied: 10×10^6 cells/mL seeding, 5 min settling time, 4 mm^2 electrodes, 3 A/mm^2 current density for 2 min to yield films 0.38 mm in thickness). To count cells, films were fixed with paraformaldehyde (2%), citrate-dissolved, then washed, resuspended, and counted via FACS. Using the electrode area and the estimated film thickness (~0.38 mm, generated at 3 A/mm^2 for 2 min; ~0.52 mm, 5 A/mm^2, 2 min) [34], we estimated an in-film volumetric cell density. The data demonstrates that "settling" time impacts in-film density; if there was no "settling" time (or an on-chip incubation period), the resultant cell density was ~3×10^6 cells/mL, much lower than the initial seeding density (10×10^6 cells/mL). Beyond 5 min the deposited cell density was typically 7×10^6 cells/mL. Indeed, there were many factors that influenced the deposited cell number: applied voltage and current density, cell number in the suspended sample, duration of the electrodeposition, etc. In addition to the "settling" time, we tested initial seeding density (Fig. 3A). Here, the deposited cell number was a strong function of initial seeding density, as one might expect. In seeding experiments with initial concentrations below 3×10^6 cells/mL, we found the resultant densities were typically concentrated by a factor of nearly 2. At the highest seed level (10×10^6 cell/mL), the opposite was observed (~30% decrease). For our purposes, a seeding density of 10×10^6 cells/mL and 5 min settling time were selected as the most convenient for creating sufficiently consistent production films. These values were used in all subsequent experiments.

Lastly, in Fig. 3A, we depict the in-film density as a function of the electrode area and deposited film thickness. These were of significant interest as a key focus of this work is its performance as the entire process and chip are shrunk in all geometric dimensions. That is, we were interested as to whether the density of entrapped cells at a production address was consistent over a variety of defined elec-

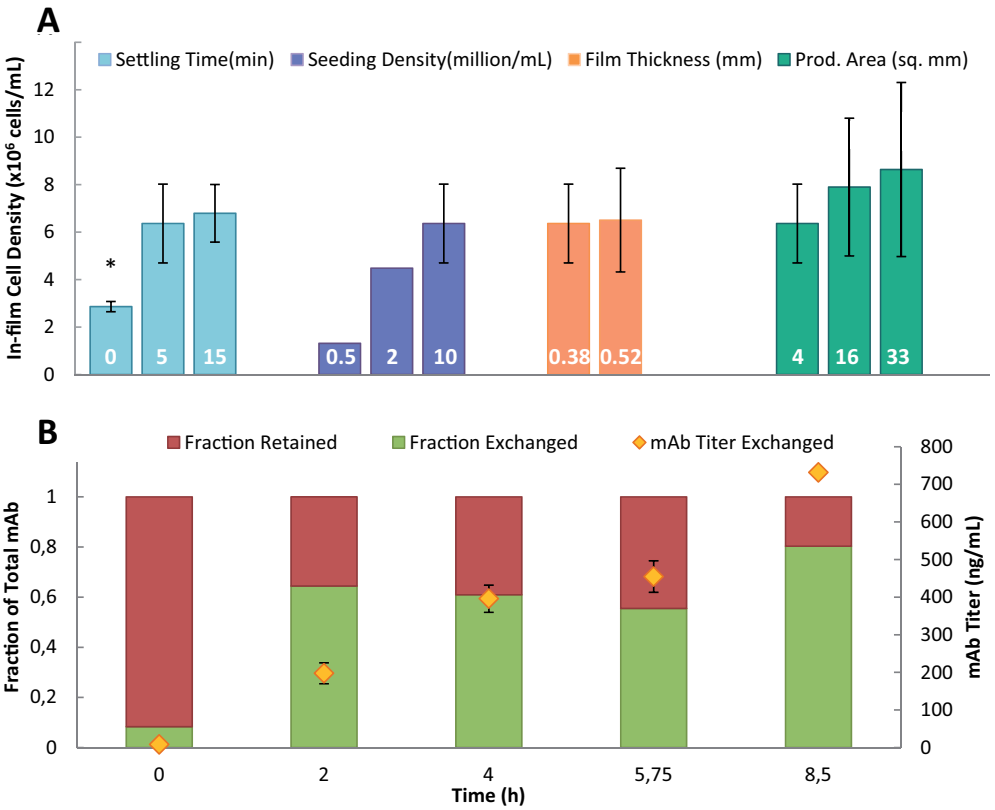

Figure 3. Characterization of the NS0 cell composition of a production address. (**A**) Electrodeposition parameters were varied to examine their effect on the resulting in-film cell density. Variation of the parameters are specified at the base of each graph and plotted against the in-film density, counted by FACS. Each variable was evaluated in at least duplicate. *$p < 0.05$. (**B**) Cells were incubated in-film for time intervals ranging from 0 to 8.5 h in order to measure mAb production over time. Titers were evaluated by the fraction detected within the alginate film and the fraction diffused, or "exchanged" from the film at regular time intervals. Titers were quantified by ELISA; the exchanged titer is reported in (**B**) in context of the fraction that it represents of total mAb produced per time.

trode areas and film thicknesses. Table 1 describes the geometries of ITO and gold electrode pairs designated for production and capture addresses, respectively. By electrode patterning, the electrode dimensions were, per pair, intrinsically set to scale (see PA/CA, Table 1). The calculated in-film cell density is shown as a function of production area size in Fig. 3A. We observed that regardless of electrode size (assuming same height/width ratios), the resulting in-film densities were nearly equivalent, with no statistical difference. Also, regardless of the electrodeposited film thickness (0.38 vs. 0.52 mm) the in-film density was constant. Our results demonstrate that adjusting deposition parameters provides some degree of control over the cellular in-film composition. We envision biofabrication at a yet smaller scale – electrodeposition on micron-sized electrodes [40]. In-film seeding, subject to the choice of parameters described here, could yield single cell entrapment for clone separation capabilities.

3.2.2 *Productivity performance: Antibody production and release from alginate hydrogels*

Electrodeposited NS0 cells were then examined for productivity when entrapped at 10×10^6 cells/mL; mAb titers were recorded as well as their distribution (within gel or secreted from gel and in the supernatant). Factors that may contribute to this distribution include the production rate and whether it is sustained [26], the crosslink density of the hydrogel network [24], and the charge density of the mAbs relative to the hydrogel (both negatively charged) [25]. Cells were codeposited into alginate films and allowed to incubate with media for 8.5 h; samples from parallel experiments were taken regularly by separately removing the extra-film media (~200 μL per test), then dissolving the film with sodium citrate (200 μL) and removing cell debris to collect the intra-film solution. The mAb levels were assayed via ELISA. In Fig. 3B, the total titer in the extra-film fluid is depicted as well as the fraction in-film and extra-film. In as little as 2 h, over 60% of the mAb was found in the extra-film fluids. This

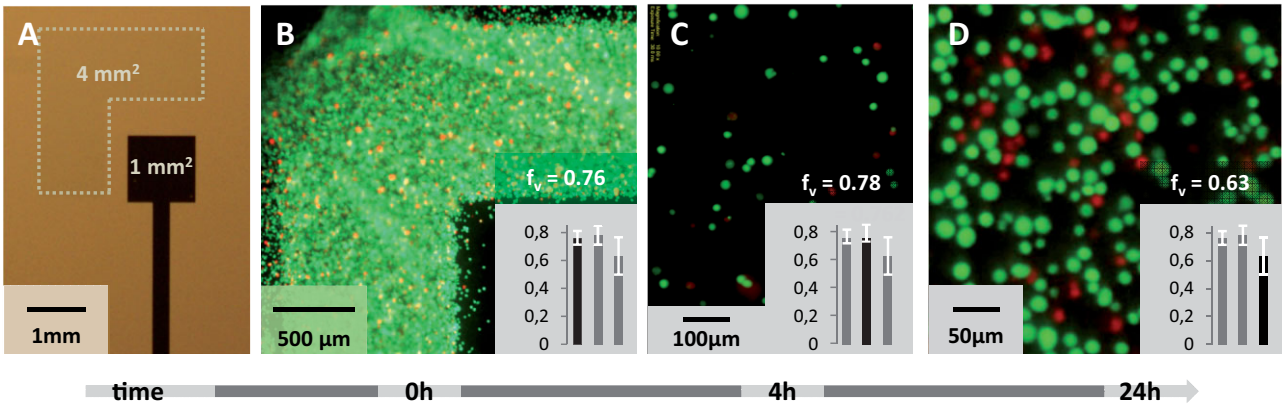

Figure 4. Cell viability during on-chip incubation and recovery. Codeposited cells were tested in triplicate for survival upon incubation in-film and recovery by film dissolution at the smallest electrode. (**A**) Electrode brightfield image. Cells stained for viability after (**B**) electrodeposition ($f_v = 0.76$), (**C**) 4 h in-film incubation and recovery (citrate dissolution, $f_v = 0.78$), and (**D**) in-film incubation, recovery, and 24 h incubation in a 96-well plate ($f_v = 0.63$). Each inset graph plots the viable fractions (f_v) and SDs for images B, C, and D, the associated data point highlighted in black.

fraction was fairly constant until 8.5 h, when the bulk (>80%) of the mAb had been diffused away. Importantly, the secreted antibody titer increased uniformly over the entire experiment, reaching 700 ng/mL at 8.5 h. These results indicate that mAbs generated and secreted at the production address may be available for capture within 2 h. As such, NS0 cells can be entrapped at a production address preserving their viability and productivity. Also, the films produced are sufficiently diffuse so that produced mAbs perfuse through the film. Cells were retained within the film and are maintained in a mAb-producing state. These results, we believe, hold promise for several applications as a means to immobilize cells and permit interactions with large molecules by diffusion into or out of the film. In addition to clonal productivity analysis, this platform could enable spatially controlled cell arrays to study metabolomics, biopsy screenings, drug targeting, or cell signaling.

3.2.3 *In-film bioprocessing utility: Incubation of entrapped NS0 cells and recovery*

Since we have observed preserved cell viability after co-deposition in an alginate film, we hypothesized that the film may serve as an adequate environment for subsequent cell incubation. Furthermore, since alginate films comprise reversible crosslinks and we have measured exceedingly high cell densities within the films, we also expected feasible cell recovery. Figure 4A shows the smallest electrode pair having dimensions of a 1 mm^2 gold electrode (capture address) and a 4 mm^2 ITO electrode (production address) used for a cell incubation and recovery study. We monitored cell survivability after co-depostion with alginate, but especially after the cells were incubated for several hours at a high density. Cell samples were concentrated to 10 × 10^6 cells/mL in 1% alginate with 0.5% $CaCO_3$. After deposition, the Live/Dead stain was applied as described. The films were imaged by fluorescence microscopy and show significant viability (Fig. 4B, $f_v = 0.76$).

Equivalent cell-entrapped films were incubated in culture media at 37°C for 4 h. After incubation, they were treated with 0.2 M sodium citrate to dissolve the films and recover the cells. Figure 4C shows cells stained for viability after incubation within a 4 mm^2 alginate film on-chip, citrate dissolution, centrifugation and resuspension steps for recovery. The majority of cells imaged were alive ($f_v = 0.78$), suggesting that the electrodeposited alginate film provides a favorable cellular microenvironment. Other samples were rinsed and recollected by centrifugation, then incubated in a 96-well plate. Figure 4D shows an image of cells recovered from a single 4 mm^2 ITO electrode and transferred to a single well for an additional 24 h incubation after residing in the alginate film. In addition to preserving their viability ($f_v = 0.63$), these cells recovered from 4 mm^2 addresses were eventually regrown to near confluency. These results suggest potential for subsequent scale up to larger cultures despite their electrodeposition and minimal sample size.

3.3 HG3T functionalized chitosan films as receptive surfaces for antibody capture

In final studies, we integrated the assembly process: a production address was assembled adjacent to a capture address, placing antibody-secreting cells in proximity to antibody-receptive HG3T, thereby allowing an opportunity for mAb ex-

Biotechnol. J. 2012, 7, 428–439

change. We evaluated capture surfaces for detectable response upon exposure to varying antibody concentrations, then their capture reliability directly from a cell sample, scalability, and semi-quantitative correlation.

3.3.1 *Capture address characterization by fluorescence analysis*

In order to ascertain whether the co-addressed cell-entrapped hydrogel would enable release and capture of antibodies (over the time span of the incubation period and after release), we first established that area-based fluorescence measurements were correlated with standard ELISA measurements. That is, human IgG at known concentrations were prepared and assayed via alkaline phosphatase based ELISA (see Section 2). For on-chip analysis, these same solutions were used as substrates for electro-assembled chitosan and enzymatically assembled HG3T capture. That is, a chitosan film was first deposited on gold, and then functionalized by applying HG3T and tyrosinase (see Section 2). Captured IgG was labeled, after incubation of the IgG solutions on-chip, with a fluorescently-conjugated $F(ab')_2$ secondary antibody fragment for fluorescence detection. Fluorescence images (Fig. 5A) were scanned using gray scale intensity measurements by examining equivalent areas of each electrode. In Fig. 5A, it was readily apparent that a monotonic increase in fluorescence with antibody titer was observed. This demonstrates success of several factors required for quantitative assessment. First, it demonstrates that the chitosan deposition and HG3T assembly processes were uniform within a particular electrode surface and, in results not depicted, repeated processing using parallel electrodes was equivalent, suggesting a robust and reproducible process.

The quantified results for each surface are depicted in Fig. 5Bi, and corresponding ELISA measurements in Fig. 5Bii. The ELISA standard curve was linear below 1000 ng/mL (r^2 = 0.99). On-chip detection of the same solutions was also linear over the same range (r^2 = 0.99). These results suggest that antibody capture using covalently assembled HG3T and detection on-chip is feasible because differences in antibody concentration can be distinguished among samples. These results also suggest the mAb capture efficiency for the on-chip method was equivalent to ELISA methods. Finally, we selected these concentrations for study as they were estimates for mAb secretion on-chip. That is, our fluorescence standard was later used to gauge the amount of mAb directly transferred from an on-chip cell population.

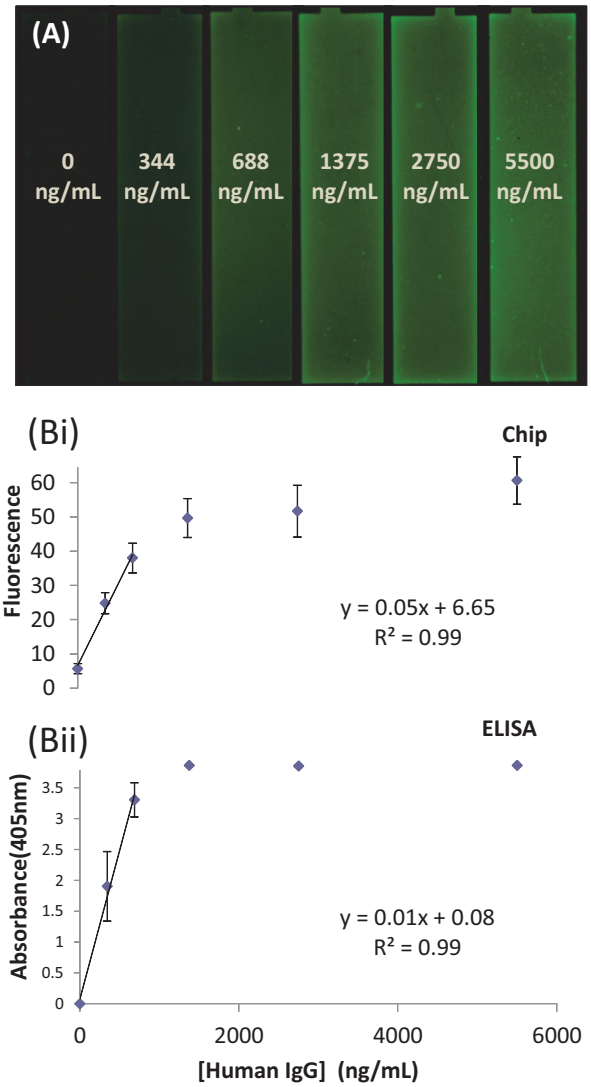

Figure 5. Fluorescence detection of captured antibody correlated to ELISA. Known concentrations of human IgG were detected by protein G-conjugated chitosan films and ELISA. (**A**) Fluorescence image of films after secondary FITC-labeling with an $F(ab')_2$ antibody. (**Bi**) Area-based fluorescence analysis of (**A**), using electrode duplicates, fluorescence intensity SD indicated by error bars. (**Bii**) Alkaline-phosphatase-based ELISA analysis, measured in triplicate with indicated SD. (**Bi**, **ii**) show linear curves below 1000 ng/mL.

3.3.2 *Receptive performance: Antibody exchange across addresses*

Transfer of mAb produced by cells incubated at the production address directly adjacent to the capture electrode was then evaluated. In this study we examined another attribute to the system that was an unanticipated benefit. Namely, the deposition of NS0 cells were suspected to increase productivity due to an artifact of increased cell density. Cell samples were taken, concentrated to 10×10^6 cells/mL, and co-deposited with alginate as described

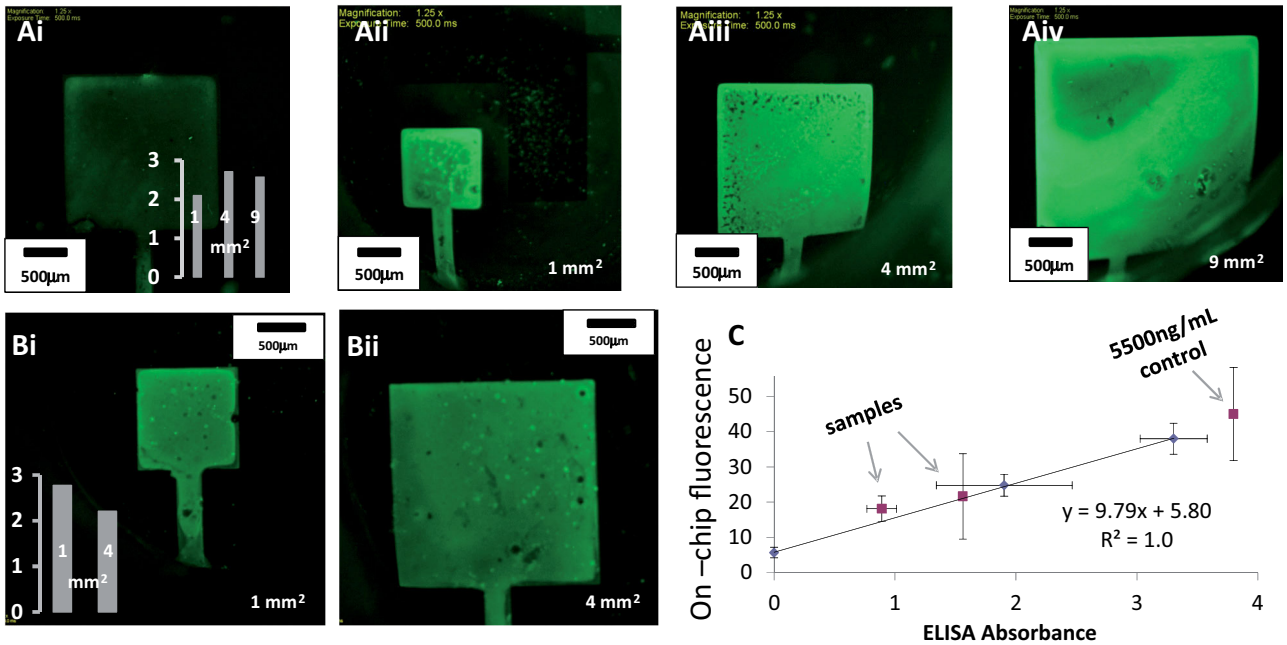

Figure 6. Scalable and quantifiable antibody exchange from production address to capture address. (**Ai**) A negative control shows capture address fluorescence due to non-specific binding of the secondary FITC-conjugated $F(ab')_2$ antibody. (**Aii–iv**) Capture addresses secondarily labeled after exposure to mAbs generated at the production address during incubation. After area-based fluorescence measurements, inset graph in (**Ai**) has been normalized to the negative control, showing fluorescence from samples as greater than twofold above the control. (**Bi, ii**) Identical samples were fluorescently probed for mAbs at the corresponding capture addresses (**Bi** – small, **Bii** – medium), with equally sized negative controls (not shown). Inset graph shows nearly equivalent fluorescence measurements normalized to the controls. (**C**) From Fig. 5(**Bi, ii**), the on-chip standard curve was plotted against that of ELISA, and detection data of two samples (mAbs diffused from production addresses) and positive control (5500 ng/mL) were semi-quantitatively measured in at least duplicate and plotted with error bars of the SD.

above. ITO electrode addresses were each paired with gold electrodes preassembled with an HG3T-functionalized chitosan film. That is, in these studies, we first created the chitosan capture surface and then assembled the production film. After deposition, the electro-addressed cell-entrapped films were incubated at 37°C for 5.5 h (see Section 2). After incubation, supernatant media were removed and hydrogels were dissolved using sodium citrate. We subsequently removed the supernatants, centrifuged the cells, and reapplied the clarified supernatant to the chips. These supernatants were incubated for 2 h for capture. Thus, the entire capture exposure time was 7.5 h, including the cell incubation time. Figure 6Aii–iv shows fluorescence images at capture addresses of each size (referring to Table 1). The fluorescence of the small, medium, and large electrodes were all significantly greater than that of a negative control (Fig 6A, normalized intensities of electrodes in Aii–iv are represented by the inset graph in Ai). Thus, we have demonstrated integrated in-film bioprocessing, where cells were entrapped and incubated and mAbs were secreted, collected, captured, and detected, all on-site, and all at distinctive millimeter-scaled addresses.

3.3.3 *Scalable relationship between addresses*

We completed identical capture studies on differently sized chips. We found that for the medium system, comprising a 4 mm^2 capture area and a 16 mm^2 production address, and over 5 h incubation, sufficiently significant mAb levels were produced, captured, and imaged. We then kept nearly the same ratio of production/capture areas (Table 1) and shrunk the entire system to contain a 1 mm^2 capture address and 4 mm^2 production address. By performing studies using identical processes and times, we show in Fig. 6Bi–ii that the level of fluorescence in the small system was nearly equivalent to that of the large system (Fig. 6B inset graph). Our results are overall consistent with the notion that the biofabricated surface construction and use is both simple and robust, but also scalable.

3.3.4 *In-film bioprocessing utility: Semi-quantification of antibody titer*

Another test probed the extra-film supernatant for released mAb during cell culture on-chip at varied incubation periods. After incubating for 2 and 4 h, we proceeded with our on-chip detection strategy. We performed gray scale quantification and also measured the supernatant via ELISA. The gray

scale quantification of the capture address' fluorescence, plotted against corresponding ELISA data, placed the antibody loading near 300 ng/mL (Fig. 6C). Importantly, the quantities were both in line with the standard curve obtained via in vitro studies. In order to verify consistency in our on-chip detection strategy, we also remeasured a positive control of 5500 ng/mL to check for correlation to standard data and found that our control closely matched (Fig. 6C). We have demonstrated success in gauging antibody presence on-chip, and have quantified its concentration.

4 Concluding remarks

This work demonstrates for the first time that biofabrication strategies can be utilized in an integrated way to electro-address multiple polysaccharide-based films for unique yet cooperative bioprocessing functions at separate yet contiguous electrode addresses. Upon cell entrapment on-chip and recovery, the functionality of an entrapped antibody-producing cell population was confirmed by on-chip detection of the secreted antibody; this is coincident with the receptive functionality maintained by HG3T after surface conjugation to capture an antibody, a metabolic product. The integration of a hydrogel-based film for non-permanent containment of a cellular component and a protein-tethered functional surface imparts new complexity in the construction of dynamic on-chip components for miniaturized bioprocesses. We suggest this approach may find the most direct utility in screening clonal populations, monitoring production runs for productivity, and for the capture of products, including other proteins, using the same technique. Furthermore, cell electrodeposition and receptor or enzyme-functionalized "biofabricated" surfaces may streamline other studies including targeting for drug delivery or signaling studies between differentiated cell populations. Ultimately, integrated biofabrication strategies may advance efforts to heighten the complexity of in vitro models.

The authors thank BioFactura, Inc. for their transfection technologies and provision of a transfectant NS0 cell line and the Maryland NanoCenter and FabLab for their facilities used toward device fabrication. They also gratefully acknowledge financial support from the US Navy ONR (N000141010446), US Army DTRA (BO085PO008), National Science Foundation EFRI program, and the R. W. Deutsch Foundation.

The authors declare no conflict of interest.

5 References

[1] Esch, M. B., King, T. L., Shuler, M. L., The role of body-on-a-chip devices in drug and toxicity studies. *Annu. Rev. Biomed. Eng.* 2011, *13*, 55–72.

[2] Sung, J. H., Yu, J., Luo, D., Shuler, M. L., March, J. C., Microscale 3-D hydrogel scaffold for biomimetic gastrointestinal (GI) tract model. *Lab Chip* 2011, *11*, 389–392.

[3] Schapper, D., Alam, M. N., Szita, N., Eliasson Lantz, A., Gernaey, K. V., Application of microbioreactors in fermentation process development: A review. *Anal. Bioanal. Chem.* 2009, *395*, 679–695.

[4] Chen, A., Chitta, R., Chang, D., Amanullah, A., Twenty-four well plate miniature bioreactor system as a scale-down model for cell culture process development. *Biotechnol. Bioeng.* 2009, *102*, 148–160.

[5] Diao, J., Young, L., Zhou, P., Shuler, M. L., An actively mixed mini-bioreactor for protein production from suspended animal cells. *Biotechnol. Bioeng.* 2008, *100*, 72–81.

[6] Rao, G., Moreira, A., Brorson, K., Disposable bioprocessing: the future has arrived. *Biotechnol. Bioeng.* 2009, *102*, 348–356.

[7] Duetz, W. A., Microtiter plates as mini-bioreactors: miniaturization of fermentation methods, *Trends Microbiol.* 2007, *15*, 469–475.

[8] Szmacinski, H., Smith, D. S., Hanson, M. A., Kostov, Y. et al., A novel method for monitoring monoclonal antibody production during cell culture. *Biotechnol. Bioeng.* 2008, *100*, 448–457.

[9] Shi, X., Lin, L. I., Chen, S. Y., Chao, S. H. et al., Real-time PCR of single bacterial cells on an array of adhering droplets. *Lab Chip* 2011, *11*, 2276–2281.

[10] Wu, W., Kang, K. T., Lee, N. Y., Bubble-free on-chip continuous-flow polymerase chain reaction: Concept and application. *Analyst* 2011, *136*, 2287–2293.

[11] Miao, J., Wu, W., Spielmann, T., Belfort, M. et al., Single-step affinity purification of toxic and non-toxic proteins on a fluidics platform. *Lab Chip* 2005, *5*, 248–253.

[12] Lai, J. J., Nelson, K. E., Nash, M. A., Hoffman, A. S. et al., Dynamic bioprocessing and microfluidic transport control with smart magnetic nanoparticles in laminar-flow devices. *Lab Chip* 2009, *9*, 1997–2002.

[13] Bareither, R., Pollard, D., A review of advanced small-scale parallel bioreactor technology for accelerated process development: Current state and future need. *Biotechnol. Prog.* 2011, *27*, 2–14.

[14] Park, T. H., Shuler, M. L., Integration of cell culture and microfabrication technology. *Biotechnol. Prog.* 2003, *19*, 243–253.

[15] Liu, Y., Kim, E., Ghodssi, R., Rubloff, G. W. et al., Biofabrication to build the biology-device interface. *Biofabrication.* 2010, *2*, 022002.

[16] Wu, L. Q., Payne, G. F., Biofabrication: Using biological materials and biocatalysts to construct nanostructured assemblies. *Trends Biotechnol.* 2004, *22*, 593–599.

[17] Chen, T. H., Small, D. A., Wu, L. Q., Rubloff, G. W. et al., Nature-inspired creation of protein-polysaccharide conjugate and its subsequent assembly onto a patterned surface. *Langmuir* 2003, *19*, 9382–9386.

[18] Wu, H. C., Shi, X. W., Tsao, C. Y., Lewandowski, A. T. et al., Biofabrication of antibodies and antigens via IgG-binding domain engineered with activatable pentatyrosine pro-tag. *Biotechnol. Bioeng.* 2009, *103*, 231–240.

[19] Shi, X. W., Tsao, C. Y., Yang, X. H., Liu, Y. et al., Electroaddressing of cell populations by co-deposition with calcium alginate hydrogels. *Adv. Funct. Mater.* 2009, *19*, 2074–2080.
[20] Cheng, Y., Luo, X., Tsao, C. Y., Wu, H. C. et al., Biocompatible multi-address 3D cell assembly in microfluidic devices using spatially programmable gel formation. *Lab Chip* 2011, *11*, 2316-2318.
[21] Koev, S. T., Dykstra, P. H., Luo, X., Rubloff, G. W. et al., Chitosan: An integrative biomaterial for lab-on-a-chip devices. *Lab Chip* 2010, *10*, 3026–3042.
[22] Sun, F., Zhitomirsky, I., Electrochemical deposition of composite biopolymer films. *Surf. Eng.* 2010, *26*, 546–551.
[23] Boccaccini, A. R., Keim, S., Ma, R., Li, Y., Zhitomirsky, I., Electrophoretic deposition of biomaterials. *J. R. Soc. Interface.* 2010, *7*, S581–S613.
[24] Yang, X. H., Kim, E., Liu, Y., Shi, X. W. et al., In-film bioprocessing and immunoanalysis with electroaddressable stimuli-responsive polysaccharides. *Adv. Funct. Mater.* 2010, *20*, 1645–1652.
[25] Selimoglu, S. M., Elibol, M., Alginate as an immobilization material for MAb production via encapsulated hybridoma cells. *Crit. Rev. Biotechnol.* 2010, *30*, 145–159.
[26] Lee, G. M., Palsson, B. O., Immobilization can improve the stability of hybridoma antibody productivity in serum-free media. *Biotechnol. Bioeng.* 1990, *36*, 1049–1055.
[27] Akerstrom, B., Brodin, T., Reis, K., Bjorck, L., Protein G: A powerful tool for binding and detection of monoclonal and polyclonal antibodies. *J. Immunol.* 1985, *135*, 2589–2592.
[28] Lee, J. M., Park, H. K., Jung, Y., Kim, J. K. et al., Direct immobilization of protein g variants with various numbers of cysteine residues on a gold surface. *Anal. Chem.* 2007, *79*, 2680–2687.
[29] Tanaka, G., Funabashi, H., Mie, M., Kobatake, E., Fabrication of an antibody microwell array with self-adhering antibody binding protein, *Anal. Biochem.* 2006, *350*, 298–303.
[30] Lewandowski, A. T., Small, D. A., Chen, T., Payne, G. F., Bentley, W. E., Tyrosine-based "activatable pro-tag": Enzyme-catalyzed protein capture and release. *Biotechnol. Bioeng.* 2006, *93*, 1207–1215.
[31] Anghileri, A., Lantto, R., Kruus, K., Arosio, C., Freddi, G., Tyrosinase-catalyzed grafting of sericin peptides onto chitosan and production of protein-polysaccharide bioconjugates. *J. Biotechnol.* 2007, *127*, 508–519.
[32] Freddi, G., Anghileri, A., Sampaio, S., Buchert, J. et al., Tyrosinase-catalyzed modification of Bombyx mori silk fibroin: Grafting of chitosan under heterogeneous reaction conditions. *J. Biotechnol.* 2006, *125*, 281–294.
[33] Chen, T., Embree, H. D., Wu, L. Q., Payne, G. F., In vitro protein-polysaccharide conjugation: tyrosinase-catalyzed conjugation of gelatin and chitosan. *Biopolymers* 2002, *64*, 292–302.
[34] Cheng, Y., Luo, X. L., Betz, J., Payne, G. F. et al., Mechanism of anodic electrodeposition of calcium alginate. *Soft Matter* 2011, *7*, 5677–5684.
[35] Braschler, T., Johann, R., Heule, M., Metref, L., Renaud, P., Gentle cell trapping and release on a microfluidic chip by in situ alginate hydrogel formation. *Lab Chip* 2005, *5*, 553–559.
[36] Wu, L. Q., Yi, H. M., Li, S., Rubloff, G. W. et al., Spatially selective deposition of a reactive polysaccharide layer onto a patterned template. *Langmuir* 2003, *19*, 519–524.
[37] Polk, A., Amsden, B., De Yao, K., Peng, T., Goosen, M. F., Controlled release of albumin from chitosan-alginate microcapsules. *J. Pharm. Sci.* 1994, *83*, 178–185.
[38] Tapia, C., Montezuma, V., Yazdani-Pedram, M., Microencapsulation by spray coagulation of diltiazem HCl in calcium alginate-coated chitosan. *AAPS PharmSciTech* 2008, *9*, 1198–1206.
[39] Dash, M., Piras, A. M., Chiellini, F., Chitosan-based beads for controlled release of proteins. in: Barbucci, Rolando.(Ed.), *Hydrogels: Biological Properties and Applications*, Springer, Milan 2009, pp. 111–120.
[40] Wu, L. Q., Lee, K., Wang, X., English, D. S. et al., Chitosan-mediated and spatially selective electrodeposition of nanoscale particles. *Langmuir* 2005, *21*, 3641–3646.

